Earth and Planetary Science Letters 621 (2023) 118398

Contents lists available at ScienceDirect

Earth and Planetary Science Letters

journal homepage: www.elsevier.com/locate/epsl

The ascent of subduction zone mélanges: Experimental constraints on mélange rock densities and solidus temperatures

Emmanuel A. Codillo [a,b,*], Veronique Le Roux [b], Benjamin Klein [c], Mark D. Behn [d], Horst R. Marschall [b,e], Gray E. Bebout [f]

[a] Massachusetts Institute of Technology/Woods Hole Oceanographic Institution Joint Program in Oceanography/Applied Ocean Science and Engineering, Woods Hole, MA 02543, USA
[b] Department of Geology and Geophysics, Woods Hole Oceanographic Institution, 266 Woods Hole Road, Woods Hole, MA 02543, USA
[c] Institute of Earth Science, University of Lausanne, Lausanne, Switzerland
[d] Department of Earth and Environmental Sciences, Boston College, Chestnut Hill, MA 02467, USA
[e] Institut für Geowissenschaften, Goethe Universität Frankfurt, Altenhöferalle 1, 60438 Frankfurt am Main, Germany
[f] Department of Earth and Environmental Sciences, Lehigh University, Bethlehem, PA 18015, USA

ARTICLE INFO

Article history:
Received 8 March 2023
Received in revised form 2 September 2023
Accepted 8 September 2023
Available online xxxx
Editor: F. Moynier

Keywords:
mélanges
melting
diapirs
subduction zones
slab-to-mantle transfer

ABSTRACT

Mélanges are mixtures of subducted materials and serpentinized mantle rocks that form along the slab-mantle interface in subduction zones. It has been suggested that mélange rocks may be able to ascend from the slab-top into the overlying mantle, as solid or partially molten buoyant diapirs, and transfer their compositional signatures to the source regions of arc magmas. However, their ability to buoyantly rise is in part tied to their phase equilibria during melting and residual densities after melt extraction, all of which are poorly constrained. Here, we report a series of piston-cylinder experiments performed at 1.5–2.5 GPa and 500–1050 °C on three natural mélange rocks that span a range of mélange compositions. Using phase equilibria, solidus temperatures, and densities for all experiments, we show that melting of mélanges is unlikely to occur along the slab-top at pressures $\leq$ 2.5 GPa, so that diapirism into the hotter mantle wedge would be required for melting to initiate. For the two metaluminous mélange compositions, diapir formation is favored up to pressures of at least 2.5 GPa. For the peraluminous mélange composition investigated, diapir buoyancy is possible at 1.5 GPa but limited at 2.5 GPa due to the formation of high-density garnet, primarily at the expense of chlorite. We also evaluate whether thermodynamic modeling (Perple_X) can accurately reproduce the phase equilibria, solidus temperatures, and density evolution of mélange compositions. Our analysis shows good agreement between models and experiments in mélange compositions with low initial water contents and low-pressure ($\leq$ 1.5 GPa) conditions. However, discrepancies between the thermodynamic models and experiments become larger at higher pressures and high-water contents, highlighting the need for an improved thermodynamic database that can model novel bulk compositions beyond the canonical subducting lithologies. This study provides experimental constraints on mélange buoyancy that can inform numerical models of mélange diapirism and influence the interpretations of both geophysical signals and geochemical characteristics of magmas in subduction zones.

1. Introduction

Subduction zones are highly dynamic regions on Earth where igneous oceanic crust, serpentinized peridotites, and sediments enter the Earth's interior and variably influence the compositions of arc magmas worldwide (Hawkesworth et al., 1993; Tera et al., 1986). The intense shearing, fluid metasomatism, and deformation processes occurring along the slab-mantle interface result in the development of mélange zones (Bebout and Barton, 2002). Field observations of exhumed high-pressure mélange rocks often display blocks of varying rock types embedded in mafic to ultramafic matrices (Bebout and Barton, 2002; Bebout, 1991; Codillo et al., 2022a; Marschall and Schumacher, 2012). Depending on metamorphic grade, these mélange matrices may include monomineralic chlorite schist, talc schist, jadeitite, and rock-types with varying amounts of amphibole, clinopyroxene, phengite, epidote, and ac-

* Corresponding author at: Earth and Planets Laboratory, Carnegie Institution for Science, Washington, District of Columbia, 20015, USA.
E-mail address: ecodillo@carnegiescience.edu (E.A. Codillo).

https://doi.org/10.1016/j.epsl.2023.118398

cessory minerals, such as titanite, rutile, ilmenite, and zircon. These hybrid rocks display a wide range of elemental and isotopic signatures reflecting distinct input lithologies and fluids, but have phase equilibria differing from those of the subducted mafic, ultramafic, and sedimentary inputs (Bebout and Barton, 2002; Codillo et al., 2022a; King et al., 2006; Marschall and Schumacher, 2012). It has been suggested that mélanges, in the form of melts or solid diapirs, may play an important role in controlling arc magma chemistry (Codillo et al., 2018; Cruz-Uribe et al., 2018; Marschall and Schumacher, 2012; Nielsen and Marschall, 2017). Whether partial melting of mélange rocks occurs along the slab-top and/or in buoyant diapirs in the mantle wedge has implications for the timing and location of elemental fractionation associated with arc magmas (Hawkesworth et al., 1997; Turner et al., 2001). For instance, chemical thermometers (*e.g.*, light rare earth elements/Ti, K_2O/H_2O, H_2O/Ce), which are used to infer the slab-top temperatures assume that the phases responsible for elemental fractionations (*e.g.*, phengite, epidote) reside at the slab-top (Hermann and Spandler, 2008; Klimm et al., 2008; Plank et al., 2009). However, if those minerals can be entrained by buoyant diapirs and/or if melting occurs in the rising diapirs, calculated temperatures would not be related to the conditions of the slab top (Cruz-Uribe et al., 2018; Marschall and Schumacher, 2012).

Geodynamic models predict that hydrated slab-top materials may become gravitationally unstable and form buoyant diapirs along a diagonal path away from the slab-top into the overlying mantle (Behn et al., 2011; Currie et al., 2007; Gerya and Yuen, 2003; Klein and Behn, 2021; Miller and Behn, 2012; Zhang et al., 2020). These buoyant diapirs transport slab components (*e.g.*, igneous crust, sediment, serpentinite, mélange rocks, and fluids) and subject them to *P-T* conditions that are otherwise unattainable along the slab-top (cf. Behn et al., 2011). These previous geodynamic studies have identified parameters such as layer thickness and composition, and slab-top geotherm to be particularly important on diapir formation and their behavior in the mantle wedge. Additionally, the presence of old xenocrystic zircon grains included within chromitite or entrained in erupted arc lavas were suggested to have been derived from subducted sediments that were transported via diapiric plumes to the base of the overlying crust (Gómez-Tuena et al., 2018; Proenza et al., 2017). Lastly, analysis of P-wave scattering in the mantle wedge indicates the presence of seismic obstructions that were interpreted as buoyant materials rising away from the slab-top (Lin et al., 2021), consistent with previous model predictions (Gerya et al., 2006).

The ability of mélange rocks to buoyantly ascend from the slab-top to the overlying mantle is tied to their phase equilibria, melting behavior, and densities. However, these processes remain poorly constrained, primarily due to a lack of experimental data on mélange compositions at the appropriate *P-T* conditions. We need to understand whether these lithologies melt along the slab-top and how the melting process affects the density of their melting residues. Mélange rocks could either ascend as diapirs that dehydrate and melt as they rise through the mantle wedge or remain at the slab-top to dehydrate and melt when subducted to greater depths.

Here we report the phase equilibria and bulk (solid + melt) and solid (solid-only) densities during melting of three natural mélange rocks collected from several exhumed high-pressure localities. We performed a series of 30 high-*P-T* melting experiments using piston cylinder apparatus at conditions relevant to subduction zone slab-top thermal structures (i.e. 500–1050 °C, 1.5–2.5 GPa) to estimate the *P-T* conditions at which mélange melting begins (solidus) and constrain the density evolution of mélange residues. Lastly, we compare how well thermodynamic models reproduce the phase equilibria and melting behavior of these novel bulk compositions and discuss the implications for mélange diapirism in subduction zones.

2. Materials and methods

To account for the compositional variability observed in exhumed high-pressure mélange rocks, we selected three natural mélange rocks as starting materials based on their mineralogy, fluid-immobile element (i.e. Cr/Al vs Al_2O_3) chemistry, and trace element chemistry (Fig. 1). Two mélange rocks from Syros, Greece (compositions SY400B and SY325, see Miller et al., 2009) and one mélange rock from Santa Catalina, USA (composition C647, see sample 6-4-7 in Bebout and Barton, 2002) were selected. These mélange rocks represent the matrices that formed by fluid-mediated mass transfer between juxtaposed mafic and ultramafic rocks in a subduction zone, for the Catalina Schist with additions and redistribution of some elements in fluids infiltrating from sedimentary sources (Bebout and Barton, 2002). The use of mélange matrix material in this study is supported by both field and geochemical evidence that they form at the expense of, and reflect contributions from their protoliths, making them representative of the composition of the mélange as a whole.

SY325 mélange is Si-Mg rich (56 wt.% and 22 wt.%, respectively) and Al-poor (2 wt.%) while SY400B mélange is Si-Al rich (50 wt.% and 17 wt.%, respectively), Mg-poor (8 wt.%). Both SY325 and SY400B have water contents of ∼3 wt.%. C647 mélange is Mg-Al rich (24 wt.% and 12 wt.%, respectively) and Si-poor (39 wt.%) with a water content of ∼8.5 wt.%. SY400B mélange displays the lowest Cr/Al and highest Al_2O_3 content, plotting closest to the mafic compositions represented by MORB (mid-ocean ridge basalt) and GLOSS (global subducting sediment) while SY325 mélange displays the highest Cr/Al and lowest Al_2O_3 content, plotting closest to the ultramafic compositions represented by DMM (depleted MORB mantle) and serpentinites. The composition of C647 mélange is intermediate between SY325 and SY400B in terms of Cr/Al and Al_2O_3 content (Fig. 1a). The normalized trace-element composition of SY400B mélange displays elevated trace-element abundances that also resemble GLOSS composition, whereas SY325 mélange displays the lowest trace-element abundances that also plot close to DMM and serpentinite compositions. The normalized trace-element composition of C647 mélange plots in between SY325 and SY400B compositions (Fig. 1b). The mineralogy and whole-rock compositions (major and trace elements) of SY325, SY400B and C647 mélanges are reported in Table S1.

Partial melting experiments were performed in a 0.5″ end-loaded solid medium piston-cylinder device at 500–1050 °C and 1.5–2.5 GPa, corresponding to a range of depths from 45 to 75 km, where a significant increase in the slab-top geotherms is predicted (Syracuse et al., 2010). Details on the experimental set-up are found in the supplementary material, and the experimental conditions and run durations are summarized in Table S2. Details on the mineralogical, textural, and compositional characterization performed on all experimental run products are described in the supplementary material.

3. Results

3.1. Approach to equilibrium

We assessed the approach to equilibrium by performing time-series experiments at the lowest temperature condition where we could identify and measure the compositions of both minerals and glassy melt pools. We conducted experiments using SY325 starting material at 1000 °C, 1.5 GPa using two run durations (96 h and 144 h) and found no significant difference (within 1 σ) in the compositions of glassy melt and mineral phases for both experiments

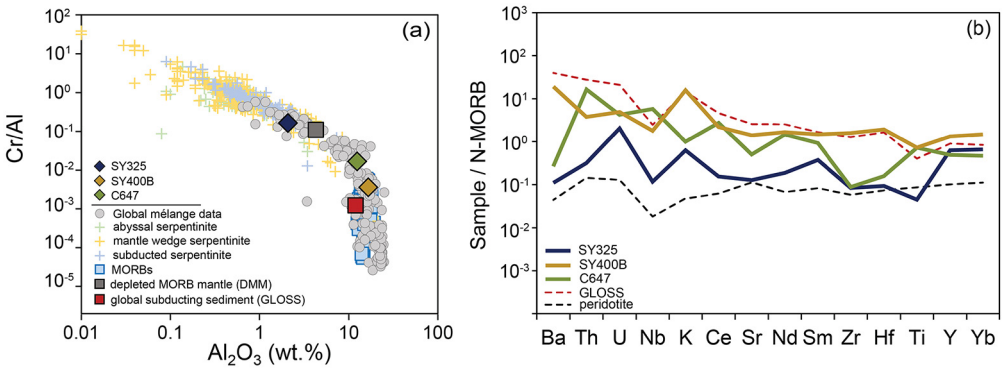

Fig. 1. Geochemical characteristics and discrimination using (a) immobile element Cr/Al vs Al_2O_3 systematics and (b) N-MORB normalized trace element compositions. The three starting mélange compositions used in this study cover a large range of the natural variability of mélanges. The N-MORB (Gale et al., 2013), normalized trace element abundances of SY325, SY400B, and C647 mélanges are plotted along with DMM-like peridotite, and GLOSS. Literature data sources: Global mélange compilation (Marschall and Schumacher, 2012), abyssal, mantle wedge and subducted serpentinite compilation (Deschamps et al., 2013), MORB compilation (Gale et al., 2013), DMM composition (Workman and Hart, 2005), and GLOSS (Plank and Langmuir, 1998). Additional information about the starting materials is available in the supplementary material.

performed at different run durations (Figure S1). Based on the likelihood of approach to equilibrium in both experiments, we selected 96 h as a minimum run duration and applied this duration to other experiments. The maintenance of a closed system during experiments and approach to equilibrium were further demonstrated by the following observations: (1) low values for the sum of residual squares ($\sum r^2$, most experiments have < 1), indicating reasonable mass balances (Tables S3–S5), (2) homogeneous distribution of minerals and melts throughout the capsule (slightly larger melt pools at the edges) and no systematic grain size variation that would suggest significant thermal gradient across the length of the capsule, (3) constancy of major element compositions in minerals and melt throughout the capsule in most experiments. An exception to this is the limited compositional zoning observed in some silicate minerals (*e.g.*, epidote and clinopyroxene in SY400B) in the lowest-temperature subsolidus experiments, likely due to slower rates of reactions under these low-temperature conditions (*e.g.*, Lakey and Hermann, 2022). Mass balance calculations in the subsolidus C647 mélange experiments at 1.5 and 2.5 GPa yielded high $\sum r^2$ (> 8) unless a free fluid phase was artificially added to the calculation. We did not measure compositions of the coexisting fluids but observed significant porosity (Fig. 5). The addition of a synthetic fluid in equilibrium with ultramafic composition of Dvir et al. (2011) in our mass-balance calculation yielded a better $\sum r^2$ (0.4–3.8) and accurately predicted mineral proportions. The near-solidus and suprasolidus experiments conducted at higher temperatures did not show any significant chemical zoning. Equilibrium attainment as reflected in good mass balances also indicated that Fe-loss was insignificant in the experiments. The modal proportions of minerals and melt for each experiment are constrained using two independent tools, Microsoft Excel Solver and LIME (Krawczynski and Olive, 2011; Prissel et al., 2023). The phase proportions (in wt.%) constrained by Solver are used in the succeeding sections after showing good agreement between the two methods (see details of the comparison in the supplementary material).

3.2. Mineral phase relations and textures

The experimental conditions and mineral phase assemblages and phase proportions are reported in Tables S3–S5 and displayed in Fig. 2. Experiments performed on SY325 mélange (~3 wt.% H_2O bulk) below the solidus are dominated by hydrous phases such as amphibole, chlorite, and talc occurring as euhedral and elongated grains that crystallized from the starting powder (Fig. 3a, b). Increased porosity in the experiments is coincident with the breakdown of chlorite and talc at temperatures below 800 °C, indicating the presence of H_2O-rich fluid phase at experimental conditions (Fig. 3c). Anthophylite is formed as a breakdown product of talc at 2.5 GPa. At near-solidus conditions, small, elongated orthopyroxene laths are observed throughout the capsule surrounding larger grains of amphibole and clinopyroxene, while interstitial melt pools are found locally around orthopyroxene grains (Fig. 3d) for both 1.5 and 2.5 GPa experiments. The solidus is constrained between 800–850 °C at 1.5 and 2.5 GPa. This is based on petrographic observation of the presence of glassy melt surrounding residual minerals. At temperatures above the solidus, the proportion of amphibole decreases until exhaustion between 900 and 1000 °C, while the proportion of orthopyroxene + clinopyroxene + melt increases and remains the stable assemblage at higher temperatures. Equant orthopyroxene and clinopyroxene grains are homogenously distributed across the length of the capsule and are surrounded by melts.

Experiments performed on SY400B mélange (~3 wt.% H_2O bulk) below the solidus are dominated by omphacitic clinopyroxene and minor amounts of phengite and chlorite that grew to form large, euhedral to subhedral grains from the starting powder. Small grains of titanite and epidote are interspersed throughout the capsule without any discernible mineral segregation textures. Accessory phases such as tourmaline, zircon, and apatite are also observed at 1.5 and 2.5 GPa. Omphacitic clinopyroxene and epidote minerals display some chemical zonation at these low-temperature subsolidus conditions (Fig. 4a, b). For instance, at 600 °C (1.5 and 2.5 GPa), clinopyroxene grains display patchy appearance in BSE images wherein the limited 'light' cores have higher FeO and lower SiO_2 and Na_2O contents than the more dominant 'dark' mantle and rims (Figure S5). The major element compositions of euhedral and chemically homogenous clinopyroxene grains in these experiments are similar to the composition of the more dominant 'dark' mantle and rims. In addition, sector zoning is observed in epidote at low-temperature subsolidus conditions. The K-rich phase is phengite at low temperature whereas phlogopite replaces phengite at higher temperatures ($\geq$ 800 °C). The solidus is constrained between 600 and 700 °C at 1.5 GPa and 700–800 °C at 2.5 GPa based on petrographic observation of the presence of glassy melt. In experiments above the solidus, hydrous melt occurs in equilibrium with diopsidic clinopyroxene + amphibole + phlogopite + titanite + epidote, and minor amounts of tourmaline, oxide, and apatite. Phlogopite and amphibole display prismatic and elongated habits surrounding larger clinopyroxene grains (Fig. 4c, d). Albitic plagioclase is the Al-rich phase at 1.5 GPa and is replaced by garnet at 2.5 GPa. Plagioclase displays prismatic habit, whereas garnet is generally equant. Rutile is commonly found in suprasolidus experiments. Melts occur as mostly dendrite-free homogenous glasses on

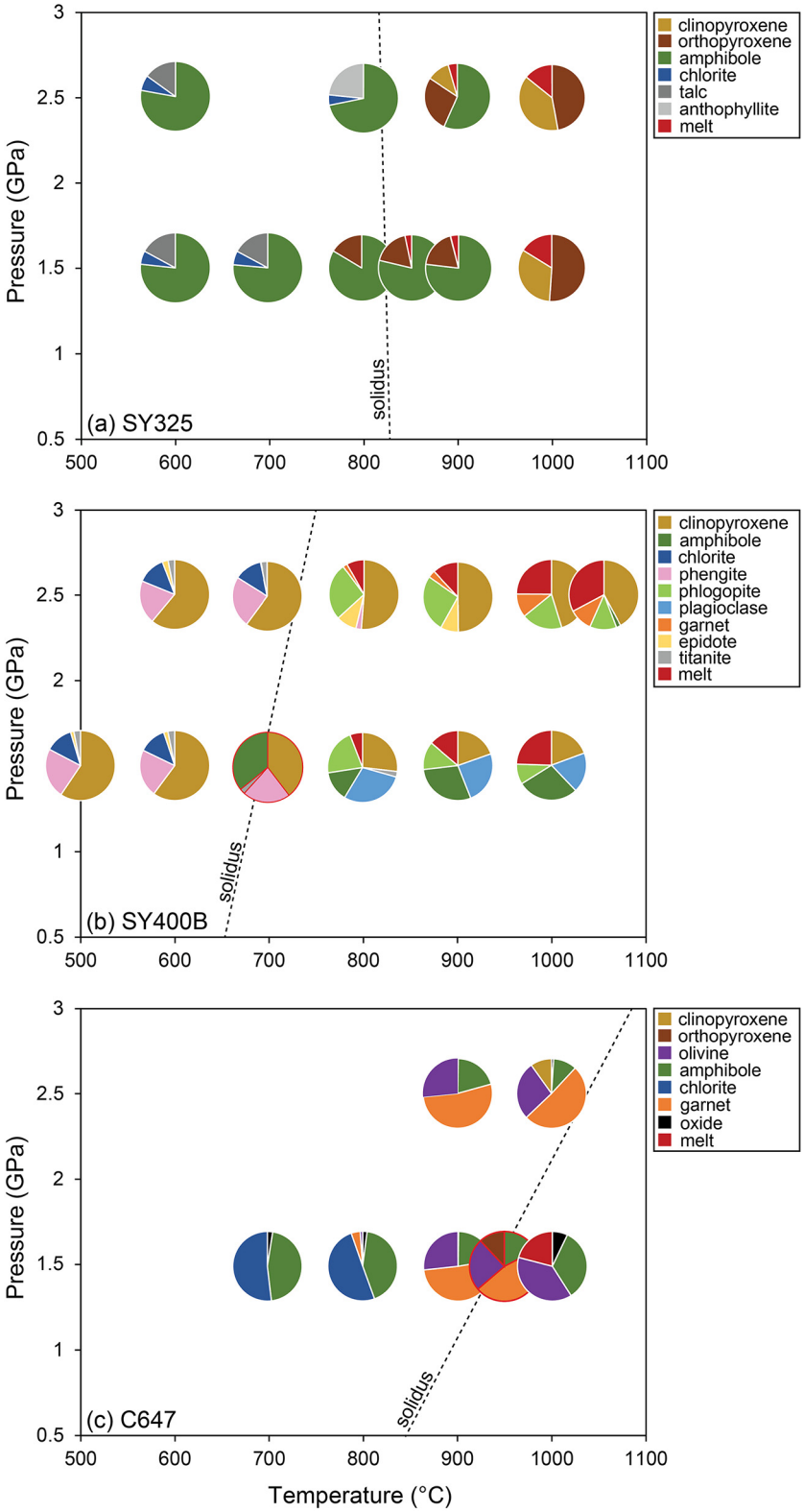

Fig. 2. Experimental conditions, phase equilibria and melting relations of (a) SY325, (b) SY400B, and (c) C647 mélanges. The solidus for each composition is shown as a dashed black line, and is an estimate (i.e., average temperature between experiments that show melt versus no melt). The mineralogy and relative proportions (in wt.%) are depicted in colored pie charts. The red margin of pie chart indicates the presence of small amounts of melts, but their compositions could not be determined due to the small size of melt pools. The phase proportions are constrained using Solver. Mineral abbreviations are from Whitney and Evans (2010).

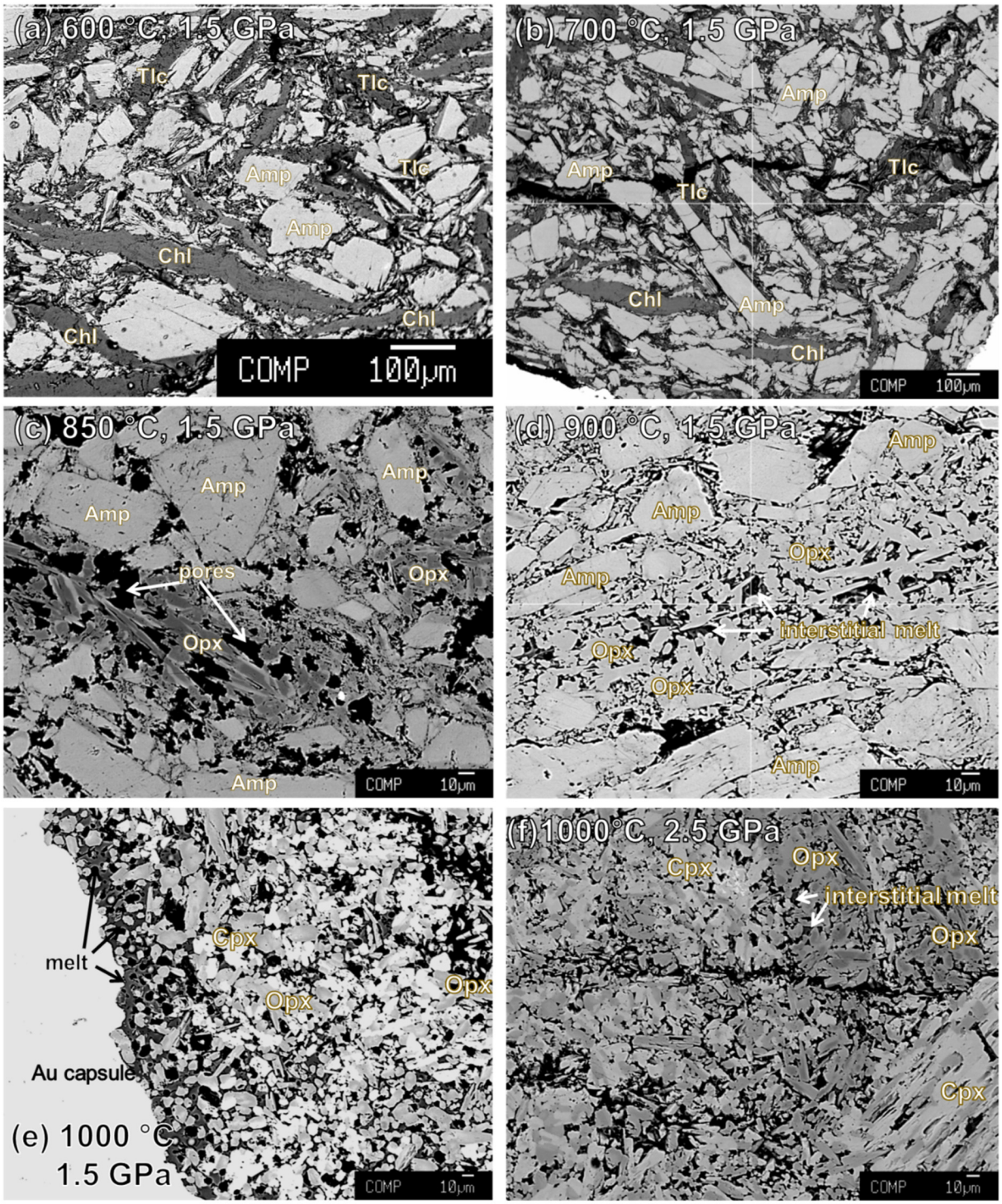

Fig. 3. Representative backscattered electron (BSE) images of SY325 experiments from subsolidus to suprasolidus conditions. (a-b) Experiments conducted below the solidus are dominated by hydrous minerals such as amphibole, chlorite and talc that display homogenous distribution in the capsule. (c-d) Breakdown of chlorite and talc leads to porosity increase with small amounts of interstitial melt. (e-f) Experiments above the solidus are dominated by anhydrous minerals orthopyroxene and clinopyroxene that are homogenously distributed in the capsule. (e) Relatively large melts pools along the capsule sides. Mineral abbreviations are from Whitney and Evans (2010).

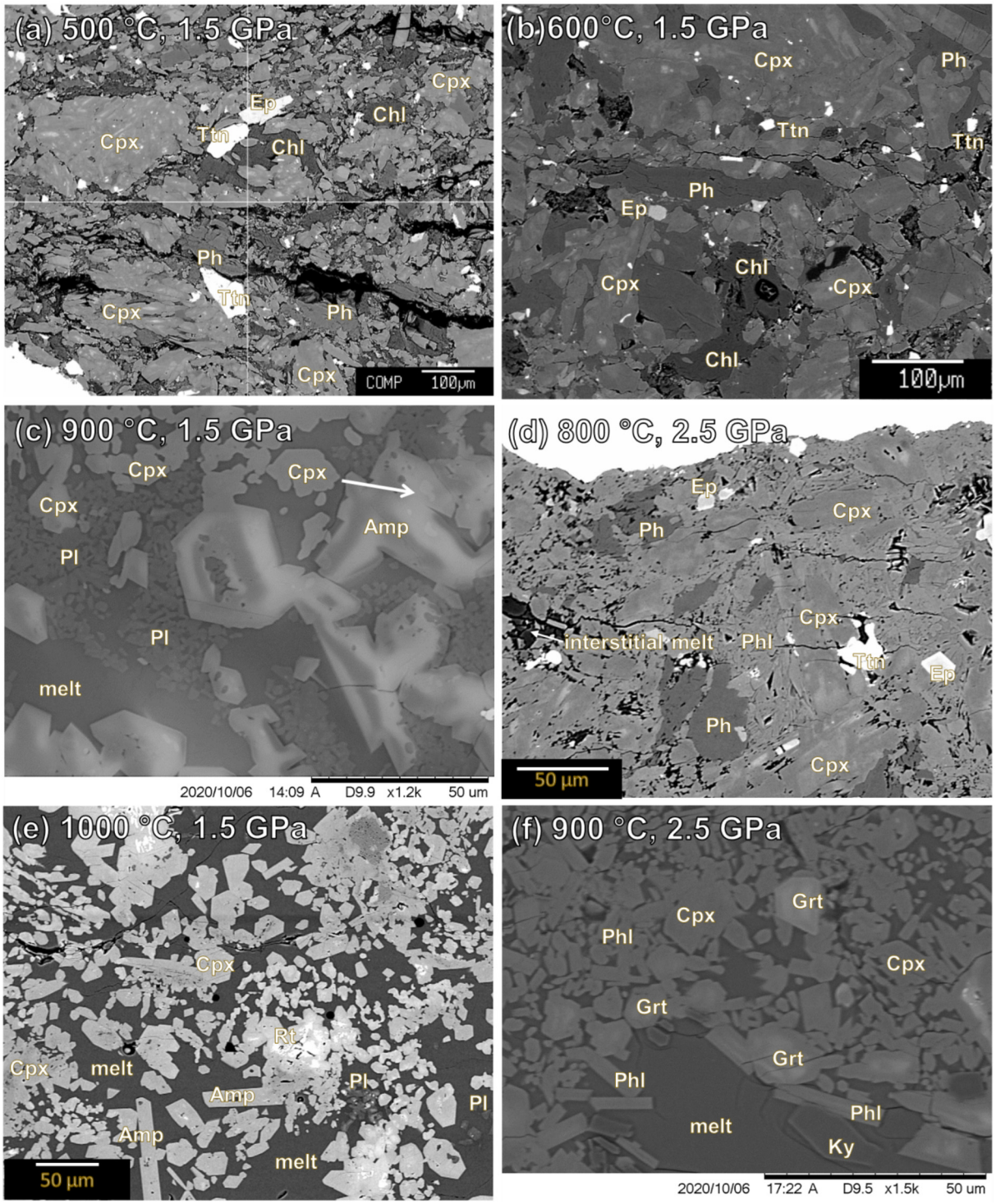

Fig. 4. Representative electron backscatter (BSE) images of SY400B experiments from subsolidus to suprasolidus conditions. (a-b) Experiments conducted below the solidus are dominated by omphacitic clinopyroxene with minor amounts of phengite and chlorite, and traces of titanite and epidote that are homogenously distributed in the capsule. Clinopyroxene and epidote minerals display chemical zonations (see Figure S5 from magnified BSE images). (c-f) Experiments above the solidus display homogenous, dendrite-free melt in equilibrium with diopsidic clinopyroxene, amphibole, phlogopite and an Al-rich phase (plagioclase at 1.5 GPa and garnet at 2.5 GPa). Traces of rutile, kyanite, and corundum are sometimes found along with melt. Mineral abbreviations are from Whitney and Evans (2010).

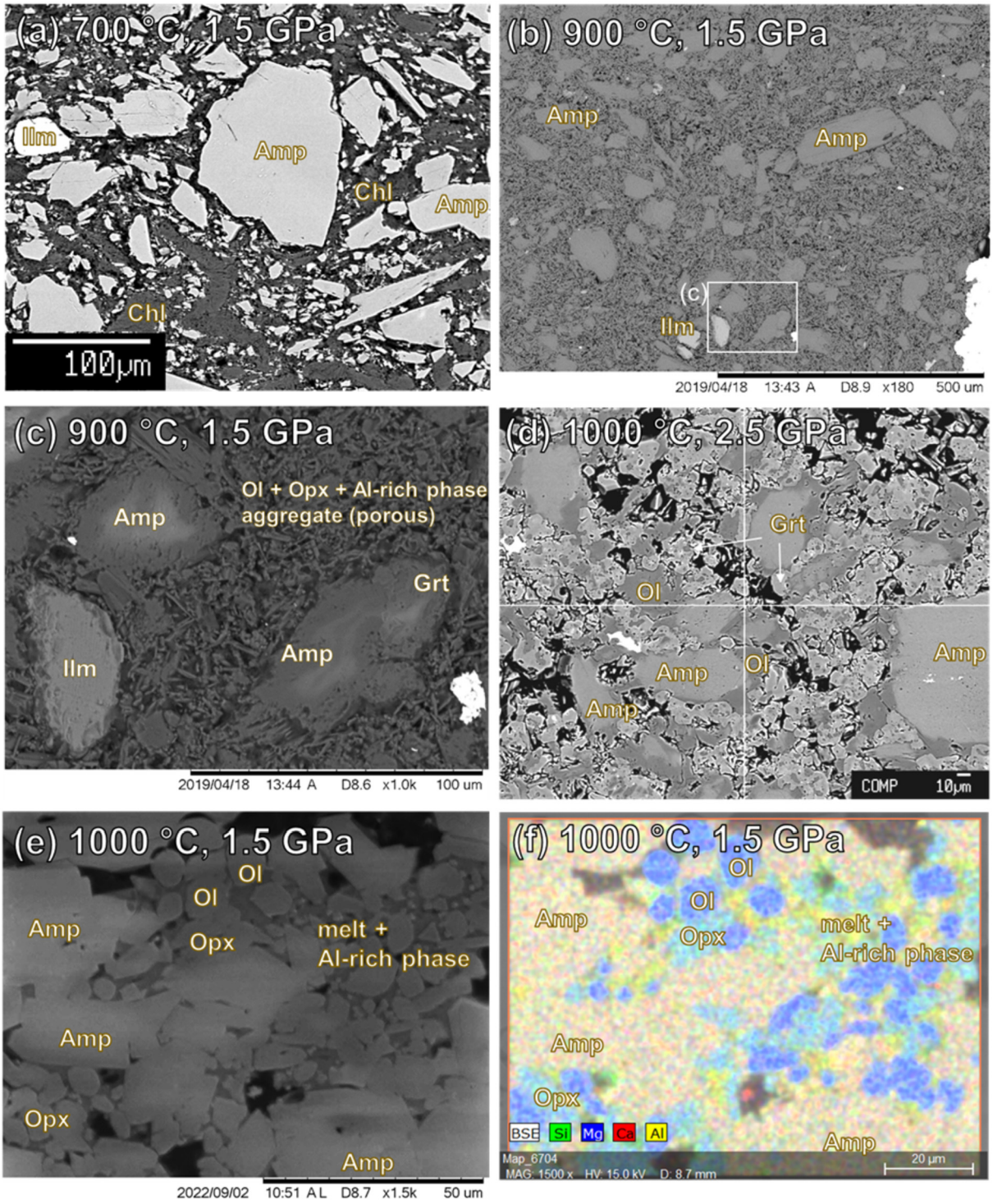

Fig. 5. Representative backscattered electron (BSE) images of C647 experiments from subsolidus to suprasolidus conditions. (a) Experiment conducted below the solidus is dominated by sub-equal proportion of amphibole and chlorite with minor ilmenite. (b-d) Subsolidus breakdown of chlorite leads to garnet formation and porosity increase partially filled with fine aggregates of olivine and minor orthopyroxene. The large porosity indicates the former presence of a H_2O-rich phase during the experiment. (e) Experiment above the solidus displays melt in equilibrium with amphibole, olivine, orthopyroxene, and minor fine-grained Al-rich phase. (f) Chemical map that display the relative concentrations of Si, Mg, Ca, and Al rastered over (e) to help identify the phases. Mineral abbreviations are from Whitney and Evans (2010).

the edges of the capsule and distributed in between mineral grains throughout the experimental run product (Fig. 4e, f).

Experiments performed on C647 (~8.5 wt.% H_2O bulk) below the solidus are dominated by sub-equal proportion of chlorite and amphibole as euhedral, elongated grains distributed across the capsule. Small grains of ilmenite are also found (Fig. 5a). At 1.5 GPa, with increasing temperature, the proportions of garnet + orthopyroxene + olivine increase, whereas the proportions of chlorite and amphibole decrease. We observed a large porosity increase in the experiment at 900 °C and 1.5 GPa, which is indicative of the presence of an H_2O-rich fluid phase at experimental conditions (Fig. 5b, c). The large amount of H_2O-rich fluid is produced

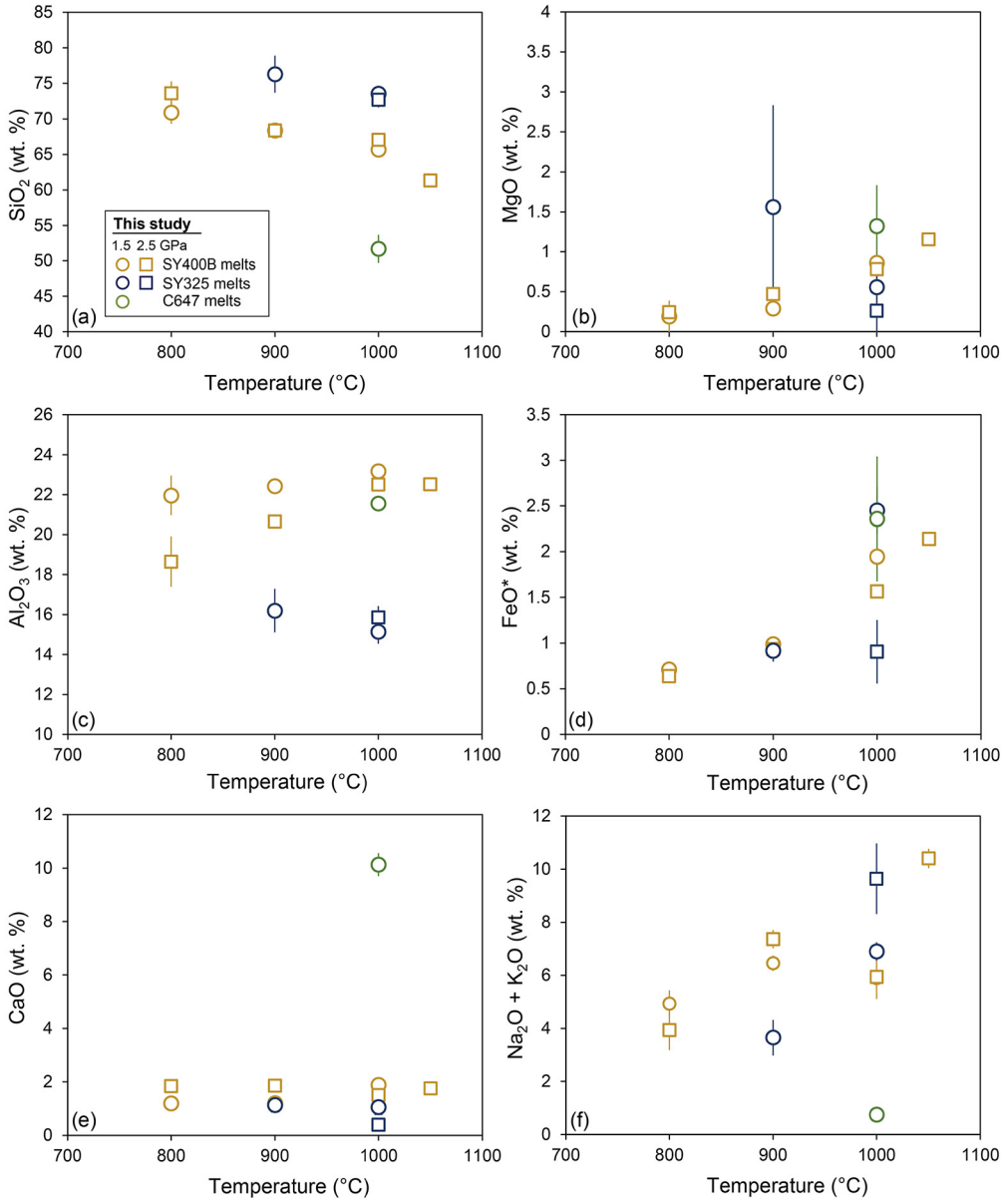

Fig. 6. Major element variations (a) SiO_2, (b) MgO, (c) Al_2O_3, (d) FeO* (as total FeO), (e) CaO, (f) $Na_2O + K_2O$ of experimental mélange melts from this study vs. temperature. Symbols: Circles are experimental melts at 1.5 GPa while squares are from 2.5 GPa. The data are plotted as averages (on volatile-free basis) with error bars representing 1 σ. When no error bars, error bars are smaller than symbols.

by the breakdown of chlorite to form fine aggregates of olivine and minor orthopyroxene at temperatures above 900 °C. The subsolidus assemblage at 2.5 GPa is dominantly composed of garnet + olivine + amphibole ± clinopyroxene. Clinopyroxene is absent in 1.5 GPa experiments but is present at 2.5 GPa. Olivine grains are euhedral to subhedral, whereas orthopyroxene and clinopyroxene are generally equant. Garnet grains commonly occur poikilitically enclosing other minerals (Fig. 5c, d). The solidus is constrained below 950 °C at 1.5 GPa whereas the solidus is not found at 2.5 GPa and therefore should be located above 1000 °C. Above the solidus, melt forms in equilibrium with olivine + orthopyroxene + amphibole ± garnet ± Al-rich phase (likely a spinel). Ilmenite is the dominant oxide phase in the experiments along with minor amounts of rutile.

3.3. Compositions of experimental melts

The average melt compositions and variations (expressed as standard deviations of the analyses) obtained using electron microprobe analyses are reported in Tables S6–S8 and displayed in Figs. 6 and S6. All experimental melts in this study are hydrous silicate melts and their compositions were measured on quenched dendrite-free glassy pools. For experiments above solidus, low-degree (< 5 wt.%) melts occurred mainly along mineral grain boundaries, whereas high-degree melts were distributed along grain boundaries and on the capsule edges (Fig. 3). Interstitial melts found in-between mineral grains are compositionally similar (within analytical uncertainty) to the larger melt pools found on capsule edges. The H_2O content of experimental melts, estimated from the difference between 100% and electron probe totals, range from ~7 to 15 wt.%. The melt H_2O contents from SY325 mélange are roughly constant at ~9 wt.%, whereas the melt H_2O contents from SY400B mélange decrease from ~15 to 6 wt.%, with increasing temperature, likely due to dilution. The melt H_2O content from C647 mélange is estimated to be ~11 wt.%. On a volatile-free basis, the melt compositions range from rhyolitic for SY325, mostly dacitic for SY400B, and a melt composition that straddles between

basalt and basaltic andesite for C647 mélange (Figure S6). The Mg# [= molar Mg/(Mg + Fe^{2+})] of all experimental melts range between 0.29–0.81.

The experimental melt compositions vary with increasing temperature at constant pressure (Fig. 6). In particular, the SiO_2 content decreases whereas Al_2O_3, FeO, MgO, and alkali contents increase with increasing temperatures in SY400B mélange experiments. The CaO content remains constant with increasing temperature and is slightly higher at higher pressure. The compositions of SY400B mélange melts did not change substantially with pressure, except for a slightly lower Al_2O_3 content in melts at higher pressure. Experimental melts of SY325 mélange display limited variations in SiO_2, Al_2O_3, MgO, and CaO contents with increasing temperature. Compared to SY400B mélange experiments, the melt compositions of SY325 mélange display significant change with pressure. At 2.5 GPa, SY325 mélange melts display systematically lower FeO and CaO contents, and higher alkali contents, whereas SiO_2, Al_2O_3, and MgO are like melts at 1.5 GPa and similar temperatures.

3.4. Compositions of experimental minerals

The mineral compositions determined using electron microprobe analyses are reported in Tables S6–S8 and are displayed in Fig. 7. In SY325 experiments, the major element compositions of amphibole, identified as actinolite (Hawthorne et al., 2012), display limited variations over the range of experimental temperatures and pressures. The Mg# of amphibole is slightly higher at 1.5 GPa (82.8–83.7) than at 2.5 GPa (82.5–82.8) at similar temperatures, with average Si and Ca contents of 7.94 a.p.f.u. (atoms per formula unit) and 1.45 a.p.f.u., respectively. The composition of orthopyroxene is rich in enstatite (En) component ranging from ~85 to 90 mol.% En. With increasing temperature at constant pressure, the orthopyroxene Mg# initially increases, from 88.9 to 90.8, then decreases to 86.7, while the average Al_2O_3 content decreases from ~3 wt.% to ~0.3 wt.%. The composition of clinopyroxene is diopsidic, with Mg# varying from 80.2 to 88.8. Chlorite and talc are both Mg-rich, with average Mg# of 83 and 93, respectively.

In SY400B experiments, the major element compositions of silicate minerals vary systematically with increasing temperature. The amphibole, which belongs to the Ca-Na and Ca groups (dominantly pargasitic and taramitic), displays a steady decrease in the average SiO_2 content with increasing temperature (Fig. 7a). The Ca content of amphibole increases with increasing temperature with amphibole displaying higher Ca contents at 1.5 GPa than at 2.5 GPa for similar experimental temperatures (Fig. 7b). The clinopyroxene composition varies from omphacitic to diopsidic with increasing temperature, with Mg# varying from ~69 to 81. The clinopyroxene displays near-constant Si content of ~2.0 a.p.f.u. followed by a drop in Si content to ~1.9 a.p.f.u. The variation in Na content in clinopyroxene mirrors the SiO_2 trend. The observed drop in Si and Na contents occurs at a temperature interval between 700 and 800 °C at 1.5 GPa and between 900 and 1000 °C at 2.5 GPa (Fig. 7c,d). The K-rich mineral in the SY400B experiments changes from phengite to phlogopite with increasing temperature (Fig. 7e, f). Phengite displays limited compositional variations at temperatures up to 800 °C, above which the average K content increases from ~1 to 1.6 a.p.f.u. Phlogopite coexists with phengite at 800 and 900 °C, but becomes the sole K-rich phase above 900 °C. The composition of plagioclase varies systematically from albitic Ab_{100} to $Ab_{66}An_{30}Or_4$, whereas the composition of garnet becomes more grossular-rich and almandine-poor from $Alm_{36}Prp_{48}Sps_2Grs_{14}$ to $Alm_{30}Prp_{47}Sps_1Grs_{22}$ with increasing temperature (Fig. 7g). Epidote displays sector zoning wherein sectors roughly show an inverse correlation in Ca and Fe contents. The Mg# of Mg-chlorite is ~80.

In C647 experiments, the amphibole displays varying composition, from magnesio-ferri-hornblende, to actinolite, to pargasite. With increasing temperature, the average SiO_2 and CaO contents initially increase at 700 °C then decrease. The composition of garnet at 1.5 GPa becomes slightly more grossular-rich and almandine-poor from $Alm_{35}Prp_{50}Sps_2Grs_{14}$ to $Alm_{24}Prp_{53}Sps_1Grs_{22}$, whereas garnet at 2.5 GPa displays limited compositional variation ($Alm_{22}Prp_{59}Sps_0Grs_{18}$ to $Alm_{21}Prp_{62}Sps_0Grs_{17}$), with increasing temperature. The average orthopyroxene Al_2O_3 content decreases with increasing temperature (Fig. 7h). The Mg# varies between 86 and 89 in clinopyroxene, and between 78 and 87 in olivine. Limited variation in Mg# is observed in Mg-chlorite and orthopyroxene with values of approximately 85 and 84, respectively.

4. Discussion

4.1. Applicability of Syros and Santa Catalina mélange matrix rocks as starting materials

A necessary precaution when interpreting the results of this study is assuring that the mineralogy and geochemical characteristics of starting materials are representative of mélange compositions that could form in situ at slab-mantle interface conditions, and not dominantly by retrograde re-equilibration at low *P-T* conditions. Our results indicate that the subsolidus assemblages at 1.5 GPa for SY325, SY400B, and C647 mélanges closely reproduced the reported thin section assemblages and modal proportions that represent equilibrium high *P-T* assemblages based on previous petrogenetic studies on these mélange rocks (Figure S7; King et al., 2006; Miller et al., 2009). In addition, the bulk-rock major element compositions of these starting materials cover a range in the compositional variability observed in global mélange compositions (Figure S8). These findings support the applicability of these natural starting materials as representative mélange compositions found along the slab-mantle interface and further imply that the compositions of our experimental melts and solid residues, as well as their densities, can be used to gain insight on subduction zone processes.

4.2. Solidi of mélange rocks

The experimentally constrained solidi for dehydration melting of the different mélange starting materials are shown in Fig. 8, along with the wet solidi for other bulk compositions (*e.g.*, sediment, basaltic igneous crust, and peridotite) relevant to subduction zone melting and a range of slab-top thermal structures. Experimental studies of fluid-saturated melting of subducting materials resulted in wet solidi between 600–700 °C at 1.5–2.5 GPa for both sediment and basaltic igneous crust compositions (Hermann and Spandler, 2008; Lambert and Wyllie, 1970; Liu et al., 1996; Nichols et al., 1994; Skora and Blundy, 2010; Till et al., 2012). We also plotted a field of wet sediment melting to account for the large compositional variability in subducting sediments. The experiments in this study were conducted on natural rock powders without the addition of excess fluid. Experimental solidi thus reflect dehydration melting with H_2O provided by the breakdown of hydrous minerals. The experiments do not constrain the fluid-saturated (or "wet") solidi for these rocks, which are potentially located at lower temperatures. The solidus for dehydration melting of SY400B mélange lies between 600–800 °C at 1.5–2.5 GPa. This solidus is comparable to wet solidi of sediment and basalt but is lower than the wet peridotite solidus at these pressures. The solidus for dehydration melting of SY325 mélange lies between 800–900 °C at 1.5–2.5 GPa. This solidus is higher than that of SY400B mélange, and higher than the wet solidi of subducted

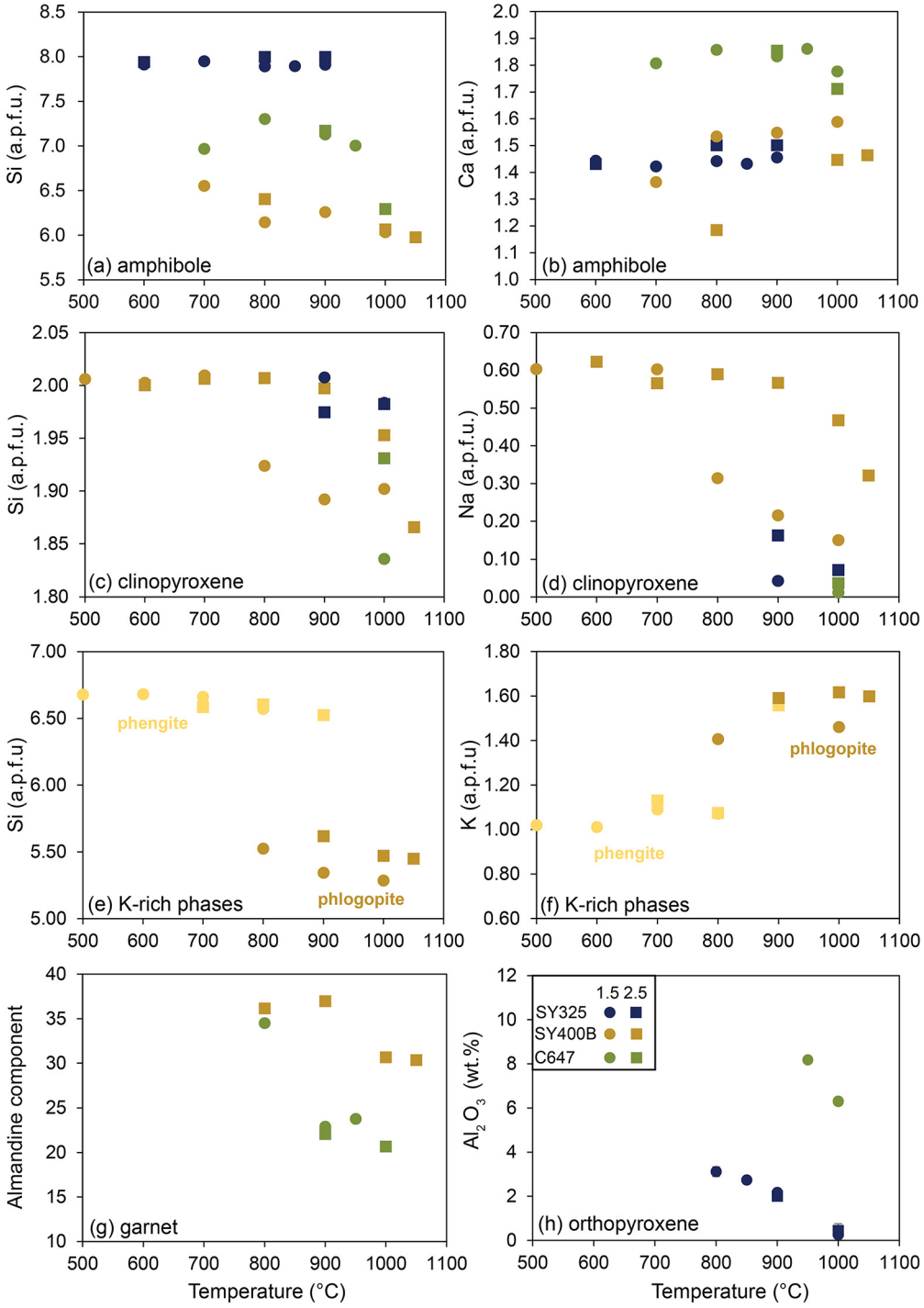

Fig. 7. Variations in the average compositions of main residual mineral phases in the experiments as functions of temperature and pressure. Blue, yellow (including light yellow for phengite), and green symbols are used for SY325, SY400B, and C647 mélange experiments, respectively. Colored circle and colored square symbols indicate minerals from 1.5 and 2.5 GPa experiments, respectively.

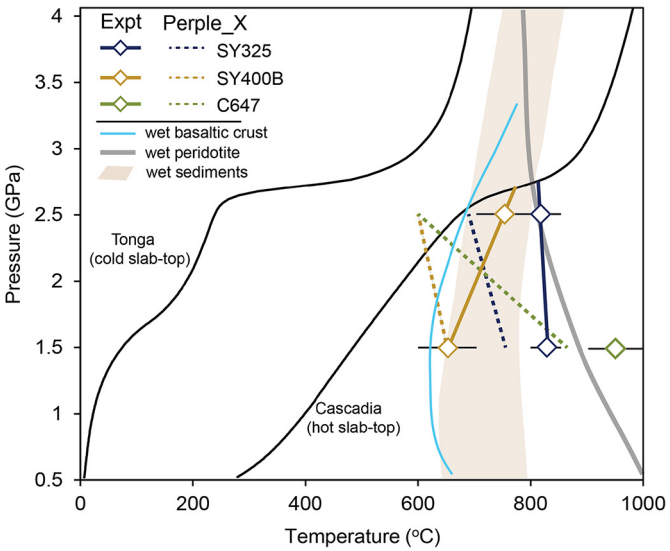

Fig. 8. Experimentally constrained solidus of different starting mélange rocks between 1.5 and 2.5 GPa. The solidi of SY400B and SY325 at pressure higher than 2.5 GPa are extrapolated by extending the traces of the solidi at 1.5 and 2.5 GPa until they intersect the warm slab-top geotherm. The solidus of C647 mélange should be located at temperature above 1000 °C at 2.5 GPa. The wet solidus of sediment, basaltic igneous crust, and peridotite, as well as the predicted solidi of mélange rocks by Perple_X model are plotted for comparison, along with slab-top geotherms representing a cold (Tonga) and a warm (Cascadia) subducting slab (D80 model of Syracuse et al., 2010). (Data references: Lambert and Wyllie, 1970; Liu et al., 1996; Mann and Schmidt, 2015; Nichols et al., 1994; Skora and Blundy, 2010; Till et al., 2012).

basalt and sediment. The solidus for dehydration melting of SY325 mélange is lower than the wet peridotite solidus at 1.5 GPa, but at 2.5 GPa it is located at higher temperature than the wet peridotite solidus. Lastly, the solidus for dehydration melting of C647 mélange lies above 900 °C at 1.5–2.5 GPa and is significantly higher than the dehydration-melting solidi of SY400B and SY325 and the wet solidi of subducted materials and peridotite at similar pressures.

If the SY325 and C647 mélanges remain along the slab-mantle interface and are entrained to greater depths, the breakdown of hydrous minerals in these mélanges can provide the necessary fluid phase to initiate wet peridotite melting. Projecting our experimentally derived solidi back to representative slab-top geotherms (Fig. 8), melting of SY325 and C647 mélanges are unlikely to occur at pressures less than 3 GPa along cold slab-tops such as in the Tonga and Mariana arcs. On the other hand, melting of SY400B and SY325 mélanges may be possible along warm slab-tops at pressures of at least 2.5 GPa, such as in the Cascadia arc. Alternatively, the high-temperature conditions needed to melt these mélange rocks may be achieved in rising diapirs into the hotter mantle wedge. The latter mechanism was suggested as an efficient mechanism necessary to extract the elemental components (*e.g.*, Th, Pb) that form the sediment-melt signature in erupted arc lavas at high-temperature conditions (> 1000 °C) (Behn et al., 2011; Syracuse et al., 2010). Therefore, for pressures at or below 2.5 GPa, melting of mélange rocks along the slab-mantle interface is unlikely. However, buoyant instabilities may form diapirs that deliver solid or partially molten mélange rocks into the hotter mantle wedge.

4.3. Slab mélange: to rise or not to rise?

The formation of buoyant diapirs from the slab-top is influenced by the density contrast between the materials along the slab-top and the overlying mantle, and densities for mélange rocks remain poorly constrained. Here, we evaluated the density contrast between mélange relative to the overlying mantle peridotites over a range of *P-T* conditions (Fig. 9). The bulk (mineral + melt) and solid (mineral-only) densities of each experimental run product were calculated from the mineral compositions and phase proportions, using the approach of Abers and Hacker (2016). In addition, melt density was calculated using the DensityX program (Iacovino and Till, 2018) while the melt viscosity was calculated using the parameterization of Giordano et al. (2008). The viscosities of hydrous mélange melts range from $10^{1.3}$–$10^{2.4}$ Pa·s for SY400B mélange, $10^{1.6}$–$10^{3.1}$ Pa·s for SY325 mélange, and $10^{1.1}$ Pa·s for C647 mélange (Table S9), well within the range of viscosities constrained for experimental anhydrous basaltic melts and hydrous sediment melts ($10^{2.5}$–$10^{-1.5}$ Pa·s) (Hack and Thompson, 2010; Schmidt, 2015). The low wetting angles (12–18°) determined for similar types of hydrous rhyolitic melts would allow for a near-instantaneous extraction of low-degree melts (Laporte, 1994). Accordingly, rapid escape of mélange partial melts upon crossing the solidus is permissible, implying that melt may not play a major role in mélange buoyancy.

The calculated bulk and solid densities from the phase proportions constrained by Solver and LIME show very good agreement (Figure S9). The calculated bulk densities (using phase proportions constrained with Solver) of subsolidus assemblages of SY400B and SY325 at 1.5–2.5 GPa are roughly constant with increasing temperature but are not for C647. At the lowest experimental temperature and 1.5 GPa, SY400B mélange displays the highest bulk density of 3180 kg/m^3, followed by SY325 and C647 mélanges with comparable bulk densities of 3000 kg/m^3 (Fig. 9). The subsolidus bulk density increases with pressure. At 2.5 GPa, the bulk density of C647 mélange increases to ~3500 kg/m^3 due to the stabilization of garnet in the subsolidus, a feature that is absent in the subsolidus assemblages of SY325 and SY400B mélanges with subsolidus bulk densities of 3050 and 3200 kg/m^3, respectively.

Melting leads to a decrease in bulk densities of SY400B and C647 mélanges whereas the opposite trend is observed for SY325 mélange. The decrease in bulk density upon melting of SY400B mélange reflects the decreased abundance of clinopyroxene and the formation of hydrous melt in equilibrium with low-density minerals such as phlogopite, plagioclase and amphibole. The decrease in bulk density in C647 mélange reflects the breakdown of garnet. In contrast, the slight increase in bulk density in SY325 mélange reflects the breakdown of dominantly amphibole to produce hydrous melt and anhydrous minerals olivine and orthopyroxene. For all the bulk compositions, the solid residue after melt extraction becomes denser, indicating that instantaneous melt extraction reduces buoyancy.

As a reference, we calculated a density range for the overlying mantle peridotite from a refractory clinopyroxene-poor harzburgite to a fertile DMM (3250–3400 kg/m^3 at 500–1100 °C and 1.5–2.5 GPa; Le Roux et al., 2014; Workman and Hart, 2005). Relative to these mantle compositions, SY325 mélange can buoyantly rise under our experimental temperatures and pressures, except at high temperatures (1000 °C and above), where the solid densities of SY325 mélange and a refractory harzburgitic mantle are similar (Figs. 9a and b). At slab-top conditions (< 700 °C,1.5–2.5 GPa; Fig. 8), a subsolidus SY325-like mélange will be able to buoyantly rise, and melting is expected to be delayed during ascent through the mantle wedge. In comparison, SY400B mélange can also buoyantly rise under experimental temperatures and pressures, except at high temperatures (1000 °C and above) at 2.5 GPa, where the solid densities of SY400B mélange and a refractory harzburgitic mantle are similar (Figs. 9c and d). At slab-top conditions, a SY400B-like mélange will be able to buoyantly rise. Because of its low solidus temperatures, melting may begin near warm slab-top conditions and continue during diapir ascent through the mantle wedge. Similarly, C647 mélange can buoyantly rise but only under lower experimental temperature and pressure conditions (< 800 °C

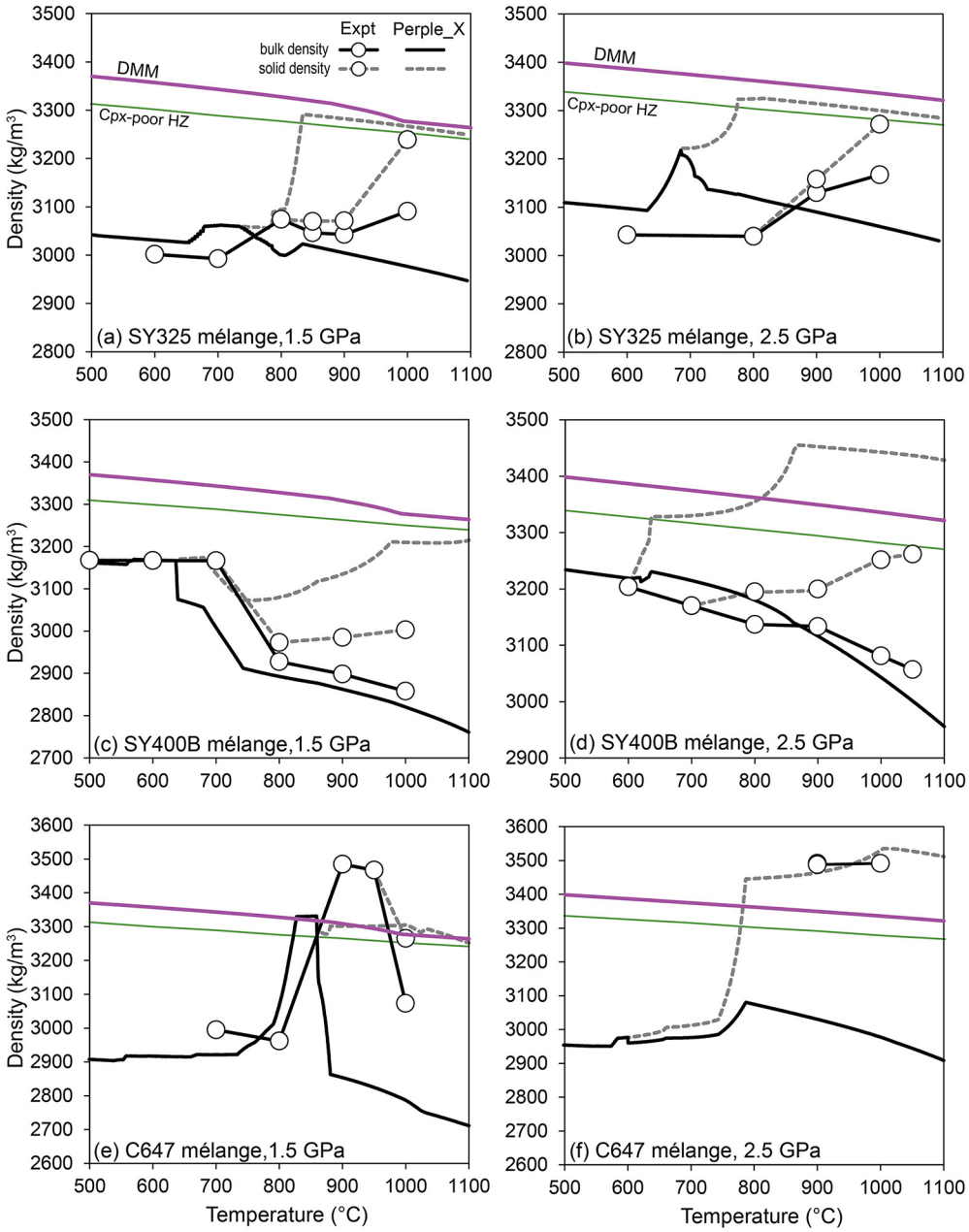

Fig. 9. Comparison of the density evolution of mélange rocks constrained by mélange melting experiments (points; this study) and thermodynamic models. Solid black lines display bulk density (residual phases + melt) while the dashed gray lines display density of solid residual phases assuming instantaneous melt extraction upon crossing the solidus. The phase proportions are constrained by Solver. As a reference, the bulk densities of depleted MORB mantle (DMM) and a more refractory clinopyroxene-poor harzburgite (Cpx-poor HZ; 71% olivine + 23% orthopyroxene + 5% clinopyroxene + 1% spinel) are plotted in solid purple and green lines, respectively. Diapirism of mélange along the slab-mantle interface is promoted when the ambient mantle is denser than mélange rocks.

and 1.5 GPa) due to the stabilization of large amounts of garnet at higher temperature and pressure conditions. At slab-top temperatures at 1.5 GPa, a subsolidus C647-like mélange will be able to buoyantly rise, and melting is expected to be delayed during ascent, occurring only in the hotter portions of the mantle wedge. Because the subsolidus assemblage of C647 mélange is significantly more dense than mantle peridotite at 2.5 GPa, buoyancy and diapirism of a C647-like mélange is unlikely at slab-top conditions. In this scenario, C647-like mélange would remain along the slab-top and be dragged to greater depths until it melts at temperatures above 1000 °C.

Using our experimental data, we can predict the fates of mélange once they have nucleated and detached from the slab-top, and begun to ascend and melt during transit into hotter portions of the wedge. Our experiments show that the subsolidus bulk densities of SY325 and SY400B mélanges at 2.5 GPa are positively buoyant relative to the overlying mantle at slab-top temperatures, thereby promoting diapir nucleation and detachment from the slab-top. In this case, diapirs that nucleated at slab-top depth (75 km) will continue to buoyantly ascend and melt extensively producing hydrous melts and residual assemblage dominated by pyroxenes, amphibole, garnet, and plagioclase, in the shallow mantle wedge.

Lakey and Hermann (2022) investigated the phase equilibria of two natural chlorite-rich lithologies (an epidote-omphacite-chlorite mélange and a monomineralic chlorite mélange) over a range of temperatures and pressures extending higher than that investigated in this study. The results showed that these mélange compo-

sitions display large jumps in bulk densities due to large amounts of subsolidus garnet formation at the expense of chlorite, like our observations in C647 mélange. They argued that this process could lead to the densification of mélange rocks relative to the overlying mantle and inhibit diapirism. We report similar results for C647 at 2.5 GPa. However, our experimental study shows that SY325 and SY400B mélanges will remain buoyant over a wide range of *P-T* conditions during subduction, and that mélanges like C647 may rise at low pressures. This study, along with the study of Lakey and Hermann (2022), highlights the importance of bulk composition in controlling the density evolution of natural mélanges and the likelihood of diapirism, especially those that favor garnet formation during prograde subduction.

Garnet is a common aluminous phase in high-pressure metamorphic rocks (*e.g.*, eclogite, metasediment). Pseudosection modeling performed on bulk compositions relevant to individual slab materials supports the more favorable garnet formation in peraluminous (pelitic) than metaluminous (basaltic) compositions with increasing *P-T* conditions during subduction (Hacker et al., 2011; Wei and Powell, 2004). Using the Alumina Saturation Index (ASI = [molar Al_2O_3/(CaO + K_2O + Na_2O)] (Nesbitt and Young, 1984)), the bulk composition of C647 is the most peraluminous (i.e. ASI > 1), followed by SY400B, and then SY325. Therefore, C647 mélange has the highest propensity to stabilize garnet early on during prograde subduction, consistent with our experimental observations. Similarly, the bulk mélange compositions used by Lakey and Hermann (2022) have ASI close to or above 1. This provides an explanation for the large amounts of subsolidus garnet in C467 mélange, as well as in the experiments of Lakey and Hermann (2022) conducted at higher pressure. On the other hand, SY400B mélange stabilized subsolidus garnet only at 2.5 GPa whereas SY325 mélange did not stabilize garnet at either 1.5 or 2.5 GPa. This implies that the compositional variability in mélanges along the slab-mantle interface and their varying response to increasing *P-T* conditions during subduction would result in density sorting that preferentially allow metaluminous bulk compositions to form diapirs.

4.4. Comparison with thermodynamic phase equilibrium models

We independently assessed the phase equilibria, modal proportions, and density evolution of the three starting compositions using the free energy minimization software Perple_X (version 6.9.1; Connolly, 2009) and appropriate thermodynamic models (dominantly from Holland et al., 2018). Details on the modeling procedure are found in the supplementary material. We calculated the phase equilibria for the same experimental bulk compositions and simulated a scenario wherein the H_2O content is fixed at a value like the bulk starting composition. In this model, a free fluid phase may or may not be present at a *P-T* condition depending on phase stability. The thermodynamically predicted solidi of the three mélange compositions all display negative slopes between 1.5 and 2.5 GPa, occurring at 750 and 690 °C for SY325, 640 and 600 °C for SY400B, and 860 and 600 °C for C647 mélange.

Comparison in the phase proportions and calculated densities between thermodynamic models and our experiments showed reasonably good agreement for SY325, SY400B, and C647 mélanges at low temperature, subsolidus conditions for both 1.5 and 2.5 GPa (Figs. 9 and S10). This also provides an independent support that our low-temperature, subsolidus experiments have closely reached chemical equilibrium. This general agreement between models and experiments is expected given that silicate mineral solution models are well-calibrated and extensively applied to investigate subsolidus (metamorphic) processes. Differences between models and experiments are more apparent at higher pressure, especially for SY325 and C647 (see discussion in the supplementary material). Models predict density change associated with mineral reactions or phase transformations at lower temperatures than indicated by experiments. Despite this offset, the models and experiments generally agree on whether mélange rocks would be buoyant relative to the overlying mantle, especially at low pressure. Models predicted higher solid density of SY400B mélange at > 3400 kg/m^3 than the overlying mantle due to the predicted garnet abundance at 2.5 GPa, at temperatures as low as 800 °C. Because the models predict extensive melting (up to 40%) of C647 mélange at temperatures below 800 °C, the resulting bulk and solid densities are significantly different from our subsolidus experiments at similar experimental *P-T* conditions.

The differences between models and experiments are unlikely to have resulted from kinetic limitation in nucleation and growth in experiments because the offset remains similar in high-temperature, suprasolidus conditions. Instead, the differences in predicted solidus temperatures and Clapeyron slopes likely reflect a limited thermodynamic database that struggles to accurately predict the phase equilibria and melting of hybrid mélange compositions, especially at elevated pressures. These findings imply that the use of phase equilibrium models (pseudosections) to assess the density evolution of mélange rocks may be a reasonably good approximation at low-temperature and low-pressure subsolidus (metamorphic) conditions for water- 'poor' mélanges (< 3 wt.% H_2O, pressures ≤ 1.5 GPa). However, we caution on the use of these models at conditions above the solidus. In this case, a better understanding of the solubility of H_2O in high-pressure mélange melts becomes crucial, highlighting the need for more experimental studies such as this one to better calibrate theoretical models at a wider range of *P-T* conditions and bulk compositions.

4.5. Potential for mélange diapirism in subduction zones

The thickness and density of the mélange layer along the slab-mantle interface will affect its overall buoyancy, while the viscosity of the layer will influence the time-scale over which the layer will become unstable and the velocity at which a diapir can ascend (Behn et al., 2011; Jull and Kelemen, 2001; Klein and Behn, 2021; Miller and Behn, 2012; Weinberg and Podladchikov, 1994). While mélange layer thicknesses in individual subduction zones are poorly constrained, conservative estimates based on field mapping of exhumed high-pressure mélange terranes are in the order of hundreds of meters to kilometer-scale (Agard et al., 2018; Bebout and Penniston-Dorland, 2016). Evaluating the viscosity contrast between the mélange layer and the overlying mantle is also difficult. This is primarily because of the lack of well-constrained rheologic flow laws for hydrous minerals, such as for chlorite, amphibole, serpentine, and mica, which comprise the bulk of mélange at low-temperature conditions. In summary, diapir initiation will occur most rapidly when the density difference between a thick mélange layer and the overlying mantle is largest, and when the viscosity of the mélange layer and overlying mantle are minimized.

The density of mélanges based on our experiments indicates that the abundance of low-density hydrous minerals such as chlorite, amphibole, talc, and mica promote a larger density contrast with the overlying mantle at low *P-T* conditions. Even though exhumed high-pressure mélange terranes display significant lithologic heterogeneity, hydrous minerals such as chlorite and amphibole are ubiquitous and in large abundance in these terranes. These observations are supported by previous studies that suggested that formation of chlorite and other hydrous minerals by fluid-mediated metasomatism of ultramafic and mafic rocks are likely pervasive along the plate interface (Bebout and Barton, 2002; Bebout, 1991; Bebout and Penniston-Dorland, 2016; Codillo et al., 2022a, 2022b). This implies that buoyancy and diapirism are possible within the thermal stability limit of chlorite at ∼850 °C (Lakey and Hermann, 2022; Pawley, 2003). Since this temperature limit

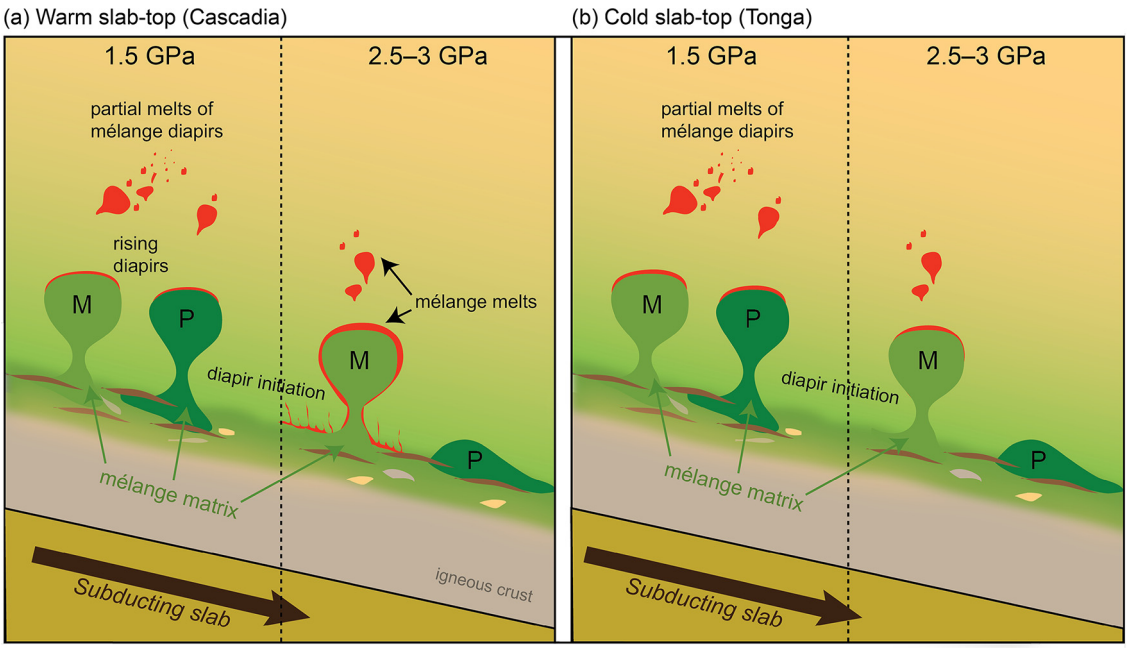

Fig. 10. Schematic cartoon that portrays the possible fates of mélange rocks along the slab-mantle interface in warm (Cascadia) and cold (Tonga) subduction zones based on this study. Mélanges display block-in matrix facies wherein blocks of sediment (yellow), igneous crust (gray), and serpentinite (brown) are embedded within mélange matrix that represent a mixture of all these components. (a) In a warm subduction zone (*e.g.*, Cascadia), the density contrast between both metaluminous (M) and peraluminous (P) mélanges and mantle wedge would allow for buoyancy-driven diapirism at relatively low pressures (1.5 GPa) and melting would not initiate at the slab top but subsequently occur later in the hotter mantle wedge during ascent. At higher pressure (2.5–3 GPa), metaluminous mélanges may undergo melting at the slab-top and may continue to melt as they rise into the hotter mantle wedge. At 2.5–3 GPa, peraluminous melanges would neither melt at the slab top, nor be able to rise as diapirs (b) In a cold subduction zone (*e.g.*, Tonga), the density contrast between both metaluminous (M) and peraluminous (P) mélanges and mantle wedge would also allow for buoyancy-driven diapirism at relatively low pressures (1.5 GPa) and melting would not initiate at the slab top but subsequently occur later in the hotter mantle wedge during ascent. At higher pressure (2.5–3 GPa), metaluminous mélanges may also be able to rise into the hotter mantle wedge, but not melt at the slab top, and undergo melting later during their ascent. At 2.5–3 GPa, peraluminous melanges would neither melt at the slab top, nor be able to rise as diapirs.

is not achieved along cold and intermediate slab-tops, and only at ~3 GPa on warm slab-tops (Syracuse et al., 2010), buoyancy and diapirism of chlorite-rich mélanges below 3 GPa would be possible for most subduction zones worldwide. However, our experimental data show that densification likely occurs upon the formation of nominally anhydrous minerals (*e.g.*, garnet and olivine) upon the breakdown of chlorite-rich assemblages (Fig. 10). Because garnet is more dense and likely more viscous than wet olivine over the range of our experimental temperatures (Hirth and Kohlstedt, 2004; Ji and Martignole, 1994; Jull and Kelemen, 2001; Shinevar et al., 2015), its formation and abundance would likely result in the stagnation of mélange residue in the mantle for peraluminous mélanges above 2.5 GPa, as has been suggested by Lakey and Hermann (2022).

5. Conclusion

This study provides an experimental assessment of the phase equilibria, melting systematics, and density evolution of mélange rocks at *P-T* conditions relevant to subduction zones. We show that melting of mélange rocks is unlikely to occur along warm or cold subducting slabs at pressures $\leq$ 2.5 GPa. Instead, our calculations suggest that, in metaluminous compositions, the density contrast between subsolidus mélange rocks and overlying mantle peridotite is sufficient to promote buoyancy and potential diapirism up to pressures of at least 2.5 GPa. The formation of garnet at 2.5 GPa in peraluminous mélange rocks likely prevents significant diapirism. Thermodynamic modeling approach can in general reproduce the subsolidus mineralogy and bulk density of the mélange rocks with low initial water contents (i.e. SY325 and SY400B) and at low-pressure conditions. However, discrepancies between models and experiments are larger at higher pressure (2.5 GPa) and for experiments with higher initial water contents, highlighting the need for an improved thermodynamic database that can better model novel bulk compositions beyond the canonical subducting lithologies. Our results suggest that buoyancy-driven ascent of mélanges into the overlying mantle may be an important and efficient process of slab-to-mantle transport of slab-derived components in subduction zones.

CRediT authorship contribution statement

Emmanuel A. Codillo: Conceptualization, Data curation, Formal analysis, Investigation, Methodology, Validation, Visualization, Writing – original draft, Writing – review & editing. **Veronique Le Roux:** Conceptualization, Funding acquisition, Methodology, Project administration, Supervision, Validation, Writing – original draft, Writing – review & editing. **Benjamin Klein:** Formal analysis, Software, Writing – review & editing. **Mark D. Behn:** Funding acquisition, Writing – review & editing. **Horst R. Marschall:** Resources, Writing – review & editing. **Gray E. Bebout:** Resources, Writing – review & editing.

Declaration of competing interest

The authors declare that they have no known competing financial interests or personal relationships that could have appeared to influence the work reported in this paper.

Data availability

All data generated and used in this study are made available in this submission

Acknowledgements

Funding for this study was supported by NSF awards EAR-P&G 1852610 to V.L.R. and EAR-P&G 1852680 to M.D.B. The authors are grateful to Dr. Ananya Mallik and Dr. Megan Guild for thoughtful and constructive comments, and Dr. Rajdeep Dasgupta for editorial handling.

Appendix A. Supplementary material

Supplementary material related to this article can be found online at https://doi.org/10.1016/j.epsl.2023.118398.

References

Abers, G.A., Hacker, B.R., 2016. A MATLAB toolbox and Excel workbook for calculating the densities, seismic wave speeds, and major element composition of minerals and rocks at pressure and temperature. Geochem. Geophys. Geosyst. 17, 616–624. https://doi.org/10.1002/2015GC006171.

Agard, P., Plunder, A., Angiboust, S., Bonnet, G., Ruh, J., 2018. The subduction plate interface: rock record and mechanical coupling (from long to short timescales). Lithos 320–321, 537–566. https://doi.org/10.1016/j.lithos.2018.09.029.

Bebout, G., Barton, M., 2002. Tectonic and metasomatic mixing in a high-T, subduction-zone mélange - Insights into the geochemical evolution of the slab-mantle interface. https://doi.org/10.1016/S0009-2541(02)00019-0.

Bebout, G.E., 1991. Field-based evidence for devolatilization in subduction zones: implications for arc magmatism. Science 251, 413. https://doi.org/10.1126/science.251.4992.413.

Bebout, G.E., Penniston-Dorland, S.C., 2016. Fluid and mass transfer at subduction interfaces—the field metamorphic record. Lithos 240–243, 228–258. https://doi.org/10.1016/j.lithos.2015.10.007.

Behn, M.D., Kelemen, P.B., Hirth, G., Hacker, B.R., Massonne, H.-J., 2011. Diapirs as the source of the sediment signature in arc lavas. Nat. Geosci. 4, 641.

Codillo, E.A., Klein, F., Dragovic, B., Marschall, H.R., Baxter, E., Scambelluri, M., Schwarzenbach, E., 2022a. Fluid-mediated mass transfer between mafic and ultramafic rocks in subduction zones. Geochem. Geophys. Geosyst. 23 (8), e2021GC010206. https://doi.org/10.1029/2021GC010206.

Codillo, E.A., Klein, F., Marschall, H.R., 2022b. Preferential formation of chlorite over talc during Si-metasomatism of ultramafic rocks in subduction zones. Geophys. Res. Lett. 49 (19), e2022GL100218. https://doi.org/10.1029/2022GL100218.

Codillo, E.A., Le Roux, V., Marschall, H.R., 2018. Arc-like magmas generated by mélange-peridotite interaction in the mantle wedge. Nat. Commun. 9, 2864. https://doi.org/10.1038/s41467-018-05313-2.

Connolly, J.A.D., 2009. The geodynamic equation of state: what and how. Geochem. Geophys. Geosyst. 10. https://doi.org/10.1029/2009GC002540.

Cruz-Uribe, A.M., Marschall, H.R., Gaetani, G.A., Le Roux, V., 2018. Generation of alkaline magmas in subduction zones by partial melting of mélange diapirs—an experimental study. Geology 46, 343–346. https://doi.org/10.1130/G39956.1.

Currie, C.A., Beaumont, C., Huismans, R.S., 2007. The fate of subducted sediments: a case for backarc intrusion and underplating. Geology 35, 1111–1114. https://doi.org/10.1130/G24098A.1.

Deschamps, F., Godard, M., Guillot, S., Hattori, K., 2013. Geochemistry of subduction zone serpentinites: a review. Lithos 178, 96–127. https://doi.org/10.1016/j.lithos.2013.05.019.

Dvir, O., Pettke, T., Fumagalli, P., Kessel, R., 2011. Fluids in the peridotite–water system up to 6 GPa and 800°C: new experimental constrains on dehydration reactions. Contrib. Mineral. Petrol. 161, 829–844. https://doi.org/10.1007/s00410-010-0567-2.

Gale, A., Dalton, C.A., Langmuir, C.H., Su, Y., Schilling, J.-G., 2013. The mean composition of ocean ridge basalts. Geochem. Geophys. Geosyst. 14, 489–518. https://doi.org/10.1029/2012GC004334.

Gerya, T.V., Connolly, J.A.D., Yuen, D.A., Gorczyk, W., Capel, A.M., 2006. Seismic implications of mantle wedge plumes. Phys. Earth Planet. Inter. 156, 59–74. https://doi.org/10.1016/j.pepi.2006.02.005.

Gerya, T.V., Yuen, D.A., 2003. Rayleigh–Taylor instabilities from hydration and melting propel 'cold plumes' at subduction zones. Earth Planet. Sci. Lett. 212, 47–62. https://doi.org/10.1016/S0012-821X(03)00265-6.

Giordano, D., Russell, J.K., Dingwell, D.B., 2008. Viscosity of magmatic liquids: a model. Earth Planet. Sci. Lett. 271, 123–134. https://doi.org/10.1016/j.epsl.2008.03.038.

Gómez-Tuena, A., Cavazos-Tovar, J.G., Parolari, M., Straub, S.M., Espinasa-Pereña, R., 2018. Geochronological and geochemical evidence of continental crust 'relamination' in the origin of intermediate arc magmas. Lithos 322, 52–66. https://doi.org/10.1016/j.lithos.2018.10.005.

Hack, A., Thompson, A., 2010. Density and viscosity of hydrous magmas and related fluids and their role in subduction zone processes. J. Petrol. 52, 1333–1362. https://doi.org/10.1093/petrology/egq048.

Hacker, B.R., Kelemen, P.B., Behn, M.D., 2011. Differentiation of the continental crust by relamination. Earth Planet. Sci. Lett. 307, 501–516. https://doi.org/10.1016/j.epsl.2011.05.024.

Hawkesworth, C.J., Gallagher, K., Hergt, J.M., McDermott, F., 1993. Mantle and slab contributions in arc magmas. Annu. Rev. Earth Planet. Sci. 21, 175–204. https://doi.org/10.1146/annurev.ea.21.050193.001135.

Hawkesworth, C.J., Turner, S.P., McDermott, F., Peate, D.W., van Calsteren, P., 1997. U-Th isotopes in arc magmas: implications for element transfer from the subducted crust. Science 276, 551. https://doi.org/10.1126/science.276.5312.551.

Hawthorne, F.C., Oberti, R., Harlow, G.E., Maresch, W.V., Martin, R.F., Schumacher, J.C., Welch, M.D., 2012. Nomenclature of the amphibole supergroup. Am. Mineral. 97, 2031–2048. https://doi.org/10.2138/am.2012.4276.

Hermann, J., Spandler, C.J., 2008. Sediment melts at sub-arc depths: an experimental study. J. Petrol. 49, 717–740. https://doi.org/10.1093/petrology/egm073.

Hirth, G., Kohlstedt, D., 2004. Rheology of the upper mantle and the mantle wedge: a view from the experimentalists. In: Inside the Subduction Factory. In: Geophysical Monograph Series, pp. 83–105.

Holland, T.J.B., Green, E.C.R., Powell, R., 2018. Melting of peridotites through to granites: a simple thermodynamic model in the system KNCFMASHTOCr. J. Petrol. 59, 881–900. https://doi.org/10.1093/petrology/egy048.

Iacovino, K., Till, C., 2018. DensityX: a program for calculating the densities of hydrous magmatic liquids from 427-1,627 °C and up to 30 kbar. Volcanica 2, 1–10. https://doi.org/10.30909/vol.02.01.0110.

Ji, S., Martignole, J., 1994. Ductility of garnet as an indicator of extremely high temperature deformation. J. Struct. Geol. 16, 985–996. https://doi.org/10.1016/0191-8141(94)90080-9.

Jull, M., Kelemen, P.B., 2001. On the conditions for lower crustal convective instability. J. Geophys. Res., Solid Earth 106, 6423–6446. https://doi.org/10.1029/2000JB900357.

King, R.L., Bebout, G.E., Moriguti, T., Nakamura, E., 2006. Elemental mixing systematics and Sr–Nd isotope geochemistry of mélange formation: obstacles to identification of fluid sources to arc volcanics. Earth Planet. Sci. Lett. 246, 288–304. https://doi.org/10.1016/j.epsl.2006.03.053.

Klein, B.Z., Behn, M.D., 2021. On the evolution and fate of sediment diapirs in subduction zones. Geochem. Geophys. Geosyst. 22, e2021GC009873. https://doi.org/10.1029/2021GC009873.

Klimm, K., Blundy, J.D., Green, T.H., 2008. Trace element partitioning and accessory phase saturation during H2O-saturated melting of basalt with implications for subduction zone chemical fluxes. J. Petrol. 49, 523–553. https://doi.org/10.1093/petrology/egn001.

Krawczynski, M.J., Olive, J.L., 2011. A new fitting algorithm for petrological mass-balance problems. In: AGU Fall Meeting Abstracts. V53B-2613.

Lakey, S., Hermann, J., 2022. An experimental study of chlorite stability in varied subduction zone lithologies with implications for fluid production, melting, and diapirism in chlorite-rich mélange rocks. J. Petrol. 63, egac029. https://doi.org/10.1093/petrology/egac029.

Lambert, I.B., Wyllie, P.J., 1970. Melting in the deep crust and upper mantle and the nature of the low velocity layer. Phys. Earth Planet. Inter. 3, 316–322. https://doi.org/10.1016/0031-9201(70)90068-3.

Laporte, D., 1994. Wetting behavior of partial melts during crustal anatexis: the distribution of hydrous silicic melts in polycrystalline aggregates of quartz. Contrib. Mineral. Petrol. 116, 486–499. https://doi.org/10.1007/BF00310914.

Le Roux, V., Dick, H.J.B., Shimizu, N., 2014. Tracking flux melting and melt percolation in supra-subduction peridotites (Josephine ophiolite, USA). Contrib. Mineral. Petrol. 168, 1064. https://doi.org/10.1007/s00410-014-1064-9.

Lin, C.-H., Shih, M.-H., Lai, Y.-C., 2021. Mantle wedge diapirs detected by a dense seismic array in Northern Taiwan. Sci. Rep. 11, 1561. https://doi.org/10.1038/s41598-021-81357-7.

Liu, J., Bohlen, S.R., Ernst, W.G., 1996. Stability of hydrous phases in subducting oceanic crust. Earth Planet. Sci. Lett. 143, 161–171. https://doi.org/10.1016/0012-821X(96)00130-6.

Mann, U., Schmidt, M.W., 2015. Melting of pelitic sediments at subarc depths: 1. Flux vs. fluid-absent melting and a parameterization of melt productivity. Chem. Geol. 404, 150–167. https://doi.org/10.1016/j.chemgeo.2015.02.032.

Marschall, H.R., Schumacher, J.C., 2012. Arc magmas sourced from mélange diapirs in subduction zones. Nat. Geosci. 5, 862–867. https://doi.org/10.1038/ngeo1634.

Miller, D.P., Marschall, H.R., Schumacher, J.C., 2009. Metasomatic formation and petrology of blueschist-facies hybrid rocks from Syros (Greece): implications for reactions at the slab–mantle interface. Lithos 107, 53–67. https://doi.org/10.1016/j.lithos.2008.07.015.

Miller, N.C., Behn, M.D., 2012. Timescales for the growth of sediment diapirs in subduction zones. Geophys. J. Int. 190, 1361–1377. https://doi.org/10.1111/j.1365-246X.2012.05565.x.

Nesbitt, H.W., Young, G.M., 1984. Prediction of some weathering trends of plutonic and volcanic rocks based on thermodynamic and kinetic considerations. Geochim. Cosmochim. Acta 48, 1523–1534. https://doi.org/10.1016/0016-7037(84)90408-3.

Nichols, G.T., Wyllie, P.J., Stern, C.R., 1994. Subduction zone melting of pelagic sediments constrained by melting experiments. Nature 371, 785–788. https://doi.org/10.1038/371785a0.

Nielsen, S.G., Marschall, H.R., 2017. Geochemical evidence for mélange melting in global arcs. Sci. Adv. 3. https://doi.org/10.1126/sciadv.1602402.

Pawley, A., 2003. Chlorite stability in mantle peridotite: the reaction clinochlore+enstatite=forsterite+pyrope+H2O. Contrib. Mineral. Petrol. 144, 449–456. https://doi.org/10.1007/s00410-002-0409-y.

Plank, T., Cooper, L.B., Manning, C.E., 2009. Emerging geothermometers for estimating slab surface temperatures. Nat. Geosci. 2, 611–615. https://doi.org/10.1038/ngeo614.

Plank, T., Langmuir, C.H., 1998. The chemical composition of subducting sediment and its consequences for the crust and mantle. Chem. Geol. 145, 325–394. https://doi.org/10.1016/S0009-2541(97)00150-2.

Prissel, K., Olive, J.-A., Krawczynski, Mi., 2023. LIME: a log-ratio-based algorithm for petrologic mass-balance problems and uncertainty assessment (0.1.0). Zenodo. https://doi.org/10.5281/zenodo.8135998.

Proenza, J.A., González-Jiménez, J.M., Garcia-Casco, A., Belousova, E., Griffin, W.L., Talavera, C., Rojas-Agramonte, Y., Aiglsperger, T., Navarro-Ciurana, D., Pujol-Solà, N., Gervilla, F., O'Reilly, S.Y., Jacob, D.E., 2017. Cold plumes trigger contamination of oceanic mantle wedges with continental crust-derived sediments: evidence from chromitite zircon grains of eastern Cuban ophiolites. Geosci. Front. https://doi.org/10.1016/j.gsf.2017.12.005.

Schmidt, M.W., 2015. Melting of pelitic sediments at subarc depths: 2. Melt chemistry, viscosities and a parameterization of melt composition. Chem. Geol. 404, 168–182. https://doi.org/10.1016/j.chemgeo.2015.02.013.

Shinevar, W.J., Behn, M.D., Hirth, G., 2015. Compositional dependence of lower crustal viscosity. Geophys. Res. Lett. 42, 8333–8340. https://doi.org/10.1002/2015GL065459.

Skora, S., Blundy, J., 2010. High-pressure hydrous phase relations of radiolarian clay and implications for the involvement of subducted sediment in arc magmatism. J. Petrol. 51, 2211–2243. https://doi.org/10.1093/petrology/egq054.

Syracuse, E.M., van Keken, P.E., Abers, G.A., 2010. The global range of subduction zone thermal models. Phys. Earth Planet. Inter. 183, 73–90. https://doi.org/10.1016/j.pepi.2010.02.004.

Tera, F., Brown, L., Morris, J., Sacks, I.S., Klein, J., Middleton, R., 1986. Sediment incorporation in island-arc magmas: inferences from 10Be. Geochim. Cosmochim. Acta 50, 535–550. https://doi.org/10.1016/0016-7037(86)90103-1.

Till, C.B., Grove, T.L., Withers, A.C., 2012. The beginnings of hydrous mantle wedge melting. Contrib. Mineral. Petrol. 163, 669–688. https://doi.org/10.1007/s00410-011-0692-6.

Turner, S., Evans, P., Hawkesworth, C., 2001. Ultrafast source-to-surface movement of melt at island arcs from ^{226}Ra-^{230}Th systematics. Science 292, 1363. https://doi.org/10.1126/science.1059904.

Wei, C., Powell, R., 2004. Calculated phase relations in high-pressure metapelites in the system NKFMASH (Na2O–K2O–FeO–MgO–Al2O3–SiO2–H2O). J. Petrol. 45, 183–202. https://doi.org/10.1093/petrology/egg085.

Weinberg, R.F., Podladchikov, Y., 1994. Diapiric ascent of magmas through power law crust and mantle. J. Geophys. Res., Solid Earth 99, 9543–9559. https://doi.org/10.1029/93JB03461.

Whitney, D.L., Evans, B.W., 2010. Abbreviations for names of rock-forming minerals. Am. Mineral. 95, 185–187. https://doi.org/10.2138/am.2010.3371.

Workman, R.K., Hart, S.R., 2005. Major and trace element composition of the depleted MORB mantle (DMM). Earth Planet. Sci. Lett. 231, 53–72. https://doi.org/10.1016/j.epsl.2004.12.005.

Zhang, N., Behn, M.D., Parmentier, E.M., Kincaid, C., 2020. Melt segregation and depletion during ascent of buoyant diapirs in subduction zones. J. Geophys. Res., Solid Earth 125, e2019JB018203. https://doi.org/10.1029/2019JB018203.